Towards a Unified Framework of Clustering-based Anomaly Detection

Zeyu Fang[1] **Ming Gu**[2] **Sheng Zhou**[1] **Jiawei Chen**[2] **Qiaoyu Tan**[3] **Haishuai Wang**[2] **Jiajun Bu**[2]

Abstract

Unsupervised Anomaly Detection (UAD) plays a crucial role in identifying abnormal patterns within data without labeled examples, holding significant practical implications across various domains. Although the individual contributions of representation learning and clustering to anomaly detection are well-established, their interdependencies remain under-explored due to the absence of a unified theoretical framework. Consequently, their collective potential to enhance anomaly detection performance remains largely untapped. To bridge this gap, in this paper, we propose a novel probabilistic mixture model for anomaly detection to establish a theoretical connection among representation learning, clustering, and anomaly detection. By maximizing a novel anomaly-aware data likelihood, representation learning and clustering can effectively reduce the adverse impact of anomalous data and collaboratively benefit anomaly detection. Meanwhile, a theoretically substantiated anomaly score is naturally derived from this framework. Lastly, drawing inspiration from gravitational analysis in physics, we have devised an improved anomaly score that more effectively harnesses the combined power of representation learning and clustering. Extensive experiments, involving 17 baseline methods across 30 diverse datasets, validate the effectiveness and generalization capability of the proposed method, surpassing state-of-the-art methods.

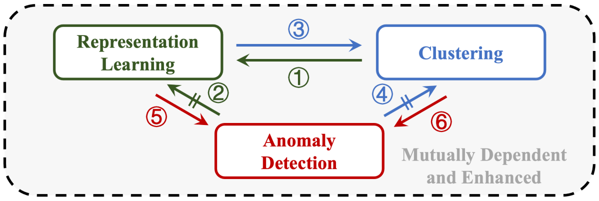

Figure 1: Interdependent relationships among representation learning, clustering, and anomaly detection.

1. Introduction

Unsupervised Anomaly Detection (UAD) refers to the task dedicated to identifying abnormal patterns or instances within data in the absence of labeled examples (Chandola et al., 2009). It has long received extensive attention in the past decades for its wide-ranging applications in numerous practical scenarios, including financial auditing (Bakumenko & Elragal, 2022), healthcare monitoring (Salem et al., 2014) and e-commerce sector (Kou et al., 2004). Due to the lack of explicit label guidance, the key to UAD is to uncover the dominant patterns that widely exist in the dataset so that samples do not conform to these patterns can be recognized as anomalies. To achieve this, early works (Chalapathy & Chawla, 2019) have heavily relied on powerful unsupervised *representation learning* methods to extract the normal patterns from high-dimensional and complex data such as images, text, and graphs. More recent works (Song et al., 2021; Aytekin et al., 2018) have utilized *clustering*, a widely observed natural pattern in real-world data, to provide critical global information for anomaly detection and achieved tremendous success.

While the individual contributions of representation learning and clustering to anomaly detection are well-established, their interrelationships remain largely unexplored. Intuitively, *discriminative representation learning* can leverage accurate clustering results to differentiate samples from distinct clusters in the embedding space (i.e., ①). Similarly, it can utilize accurate anomaly detection to avoid preserving abnormal patterns (i.e., ②). For *accurate clustering*, it can gain advantages from representation learning by operating in the discriminative embedding space (i.e., ③). Meanwhile, it can potentially benefit from accurate anomaly detection by excluding anomalies when formulating clusters (i.e., ④). *Anomaly detection* can greatly benefit from both discriminative representation learning and accurate clustering (i.e., ⑤ & ⑥). However, these benefits hinge on the successful identification of anomalies and the reduction of their detri-

[1]Zhejiang Key Laboratory of Accessible Perception and Intelligent Systems, Zhejiang University, Hangzhou, China [2]The State Key Laboratory of Blockchain and Data Security, Hangzhou, China [3]New York University Shanghai, Shanghai, China. Correspondence to: Sheng Zhou <zhousheng_zju@zju.edu.cn>.

Proceedings of the 42^{nd} International Conference on Machine Learning, Vancouver, Canada. PMLR 267, 2025. Copyright 2025 by the author(s).

mental impact on the aforementioned tasks. As depicted in Figure 1, the integration of these three elements exhibits a significant reciprocal nature. In summary, representation learning, clustering, and anomaly detection are interdependent and intricately intertwined. Therefore, it is crucial for anomaly detection to *fully leverage and mutually enhance the relationships among these three components*.

Despite the intuitive significance of the interactions among representation learning, clustering, and anomaly detection, existing methods have only made limited attempts to exploit them and fall short of expectations. On one hand, some methods (Zong et al., 2018) have acknowledged the interplay among these three factors, but their focus remains primarily on the interactions between two factors at a time, making only targeted improvements. For instance, some strategies include explicitly removing outlier samples during the clustering process (Chawla & Gionis, 2013) or designing robust representation learning methods (Cho et al., 2021) to mitigate the influence of anomalies. On the other hand, recent methods (Song et al., 2021) have begun to explore the simultaneous optimization of these three factors within a single framework. However, these attempts are still in the stage of merely superimposing the objectives of the three factors without a unified theoretical framework. This lack of a guiding framework prevents the adequate modeling of the interdependencies among these factors, thereby limiting their collective contribution to a unified anomaly detection objective. Consequently, we aim to address the following question: *Is it possible to employ a unified theoretical framework to jointly model these three interdependent objectives, thereby leveraging their respective strengths to enhance anomaly detection?*

In this paper, we try to answer this question and propose a novel model named UniCAD for anomaly detection. The proposed UniCAD integrates representation learning, clustering, and anomaly detection into a unified framework, achieved through the theoretical guidance of maximizing the anomaly-aware data likelihood. Specifically, we explicitly model the relationships between samples and multiple clusters in the representation space using the probabilistic mixture models for the likelihood estimation. Moreover, we creatively introduce a learnable indicator function into the objective of maximum likelihood to explicitly attenuate the influence of anomalies on representation learning and clustering. Under this framework, we can theoretically derive an anomaly score that indicates the abnormality of samples, rather than heuristically designing it based on clustering results as existing works do. Furthermore, building upon this theoretically supported anomaly score and inspired by the theory of universal gravitation, we propose a more comprehensive anomaly metric that considers the complex relationships between samples and multiple clusters. This allows us to better utilize the learned representations and clustering results from this framework for anomaly detection. We conduct extensive experiments with 15 baselines on 30 datasets from different data domains to evaluate the effectiveness of the proposed method. The results verify the effectiveness and generalization capability in detecting anomalies in real-world applications.

To sum up, we underline our contributions as follows:

- We propose a unified theoretical framework to jointly optimize representation learning, clustering, and anomaly detection, allowing their mutual enhancement and aid in anomaly detection.
- Based on the proposed framework, we derive a theoretically grounded anomaly score and further introduce a more comprehensive score with the vector summation, which fully releases the power of the framework for effective anomaly detection.
- Extensive experiments have been conducted on 30 datasets to validate the superior unsupervised anomaly detection performance of our approach, which surpassed the state-of-the-art through comparative evaluations with 17 baseline methods.

2. Related Work

Various UAD methods have been proposed based on different assumptions, making them suitable for detecting various types of anomaly patterns, including subspace-based models (Kriegel et al., 2009), statistical models (Goldstein & Dengel, 2012), linear models (Wold et al., 1987; Manevitz & Yousef, 2001), density-based models (Breunig et al., 2000; Peterson, 2009), ensemble-based models (Pevnỳ, 2016; Liu et al., 2008), probability-based models (Reynolds et al., 2009; Zong et al., 2018; Li et al., 2022; 2020), representation-based models (Ruff et al., 2018; Xu et al., 2023; Goyal et al., 2020; Qiu et al., 2021), and cluster-based models (He et al., 2003; Chawla & Gionis, 2013). Considering the field of anomaly detection has progressed by integrating clustering information to enhance detection accuracy (Li et al., 2021; Zhou et al., 2022), we primarily focus on and analyze anomaly patterns related to clustering, incorporating a global clustering perspective to assess the degree of anomaly. Notable methods in this context include CBLOF (He et al., 2003), which evaluates anomalies based on the size of the nearest cluster and the distance to the nearest large cluster. Similarly, DCFOD (Song et al., 2021) introduces innovation by applying the self-training architecture of the deep clustering (Xie et al., 2016) to outlier detection. Meanwhile, DAGMM (Zong et al., 2018) combines deep autoencoders with Gaussian mixture models, utilizing sample energy as a metric to quantify the anomaly degree. In contrast, our approach introduces a unified theoretical framework that integrates representation learning, clustering, and anomaly detection, overcoming the limitations of heuristic designs and the overlooked anomaly influence in existing methods.

3. Methodology

In this section, we first define the problem we studied and the notations used in this paper. Then we elaborate on the proposed method UniCAD. More specifically, we first introduce a novel learning objective that optimizes representation learning, clustering, and anomaly detection within a unified theoretical framework by maximizing the data likelihood. A novel anomaly score with theoretical support is also naturally derived from this framework. Then, inspired by the concept of universal gravitation, we further propose an enhanced anomaly scoring approach that leverages the intricate relationship between samples and clustering to detect anomalies effectively. Finally, we present an efficient iterative optimization strategy to optimize this model and provide a complexity analysis for the proposed model in Appendix D.4.

Definition 1 (Unsupervised Anomaly Detection)**.** *Given a dataset $\mathbf{X} \in \mathbb{R}^{N\times D}$ comprising N instances with D-dimensional features, unsupervised anomaly detection aims to learn an anomaly score o_i for each instance $\mathbf{x}_i$ in an unsupervised manner so that the abnormal ones have higher scores than the normal ones.*

3.1. Maximizing Anomaly-aware Likelihood

Previous research has demonstrated the importance of discriminative representation and accurate clustering in anomaly detection (Song et al., 2021). However, the presence of anomalous samples can significantly disrupt the effectiveness of both representation learning and clustering (Duan et al., 2009). While some existing studies have attempted to integrate these three separate learning objectives, the lack of a unified theoretical framework has hindered their mutual enhancement, leading to suboptimal results.

To tackle this issue, in this paper, we propose a unified and coherent approach that considers representation learning, clustering, and anomaly detection by maximizing the likelihood of the observed data. Specifically, we denote the parameters of representation learning as Θ, the clustering parameter as Φ, and the dynamic indicator function for anomaly detection as $\delta(\cdot)$. These parameters are optimized simultaneously by maximizing the likelihood of the observed data $\mathbf{X}$:

$$\begin{aligned}
&\max \log p(\mathbf{X}|\Theta, \Phi) \\
&= \max \sum_{i=1}^{N} \delta(\mathbf{x}_i) \log p(\mathbf{x}_i|\Theta, \Phi) \\
&= \max \sum_{i=1}^{N} \delta(\mathbf{x}_i) \log \sum_{k=1}^{K} p(\mathbf{x}_i, c_i = k|\Theta, \Phi),
\end{aligned} \tag{1}$$

where c_i represents the latent cluster variable associated with $\mathbf{x}_i$, and $c_i = k$ denotes the probabilistic event that $\mathbf{x}_i$ belongs to the k-th cluster. The $\delta(\mathbf{x}_i)$ is an indicator function that determines whether a sample $\mathbf{x}_i$ is an anomaly of value 0 or a normal sample of value 1.

3.1.1. Joint Representation Learning and Clustering with $p(\mathbf{x}_i|\Theta, \Phi)$

Based on the aforementioned advantages of MMs, we estimate the likelihood $p(\mathbf{x}_i|\Theta, \Phi)$ with mixture models defined as:

$$\begin{aligned}
p(\mathbf{x}_i|\Theta, \Phi) &= \sum_{k=1}^{K} p(\mathbf{x}_i, c_i = k|\Theta, \Phi) \\
&= \sum_{k=1}^{K} p(c_i = k) \cdot p(\mathbf{x}_i|c_i = k, \Theta, \boldsymbol{\mu}_k, \Sigma_k) \\
&= \sum_{k=1}^{K} \omega_k \cdot p(\mathbf{x}_i|c_i = k, \Theta, \boldsymbol{\mu}_k, \Sigma_k),
\end{aligned} \tag{2}$$

where $\Phi = \{\omega_k, \boldsymbol{\mu}_k, \Sigma_k\}$. The mixture model is parameterized by the prototypes $\boldsymbol{\mu}_k$, covariance matrices Σ_k, and mixture weights ω_k from all clusters. $\sum_{k=1}^{K} \omega_k = 1$, and $k = 1, 2, \cdots, K$.

In practice, the samples are usually attributed to high-dimensional features and it is challenging to detect anomalies from the raw feature space (Ruff et al., 2021). Therefore, modern anomaly detection methods (Ruff et al., 2018; Zong et al., 2018) often map raw data samples $\mathbf{X} = \{\mathbf{x}_i\} \in \mathbb{R}^{N\times D}$ into a low-dimensional representation space $\mathbf{Z} = \{\mathbf{z}_i\} \in \mathbb{R}^{N\times d}$ with a representation learning function $\mathbf{z}_i = f_\Theta(\mathbf{x}_i)$ and detect anomalies within this latent representation space.

Following this widely adopted practice, we model the distribution of samples in the latent representation space with a multivariate Student's-t distribution giving its cluster $c_i = k$. The Student's-t distribution is robust against outliers due to its heavy tails. Bayesian robustness theory leverages such distributions to dismiss outlier data, favoring reliable sources, making the Student's-t process preferable over Gaussian processes for data with atypical information (Andrade, 2023). Thus the probability distribution of generating

$\mathbf{x}_i$ with latent representation $\mathbf{z}_i$ given its cluster $c_i = k$ can be expressed as:

$$\begin{aligned} & p(\mathbf{x}_i | c_i = k, \Theta, \boldsymbol{\mu}_k, \Sigma_k) \\ & = \frac{\Gamma(\frac{\nu+1}{2}) |\Sigma_k|^{-1/2}}{\Gamma(\frac{\nu}{2}) \sqrt{\nu\pi}} \left(1 + \frac{1}{\nu} D_M(\mathbf{z}_i, \boldsymbol{\mu}_k)^2 \right)^{-\frac{\nu+1}{2}}, \end{aligned} \tag{3}$$

where $\mathbf{z}_i = f_\Theta(\mathbf{x}_i)$ denotes the representation obtained from the data mapped through the neural network parameterized by Θ. Γ denotes the gamma function while ν is the degree of freedom. Σ_k is the scale parameter. $D_M(\mathbf{z}_i, \boldsymbol{\mu}_k) = \sqrt{(\mathbf{z}_i - \boldsymbol{\mu}_k)^T \Sigma_k^{-1} (\mathbf{z}_i - \boldsymbol{\mu}_k)}$ represents the Mahalanobis distance (McLachlan, 1999). In the unsupervised setting, as cross-validating ν on a validation set or learning it is unnecessary, ν is set as 1 for all experiments (Xie et al., 2016; Van Der Maaten, 2009). The overall marginal likelihood of the observed data $\mathbf{x}_i$ can be simplified as:

$$p(\mathbf{x}_i | \Theta, \Phi) = \sum_{k=1}^{K} \omega_k \cdot \frac{\pi^{-1} \cdot |\Sigma_k|^{-1/2}}{1 + D_M(\mathbf{z}_i, \boldsymbol{\mu}_k)^2}. \tag{4}$$

3.1.2. Anomaly Indicator $\delta(\mathbf{x}_i)$ and Score o_i

As we have discussed, the indicator function $\delta(\mathbf{x}_i)$ not only benefits both representation and clustering but also directly serves as the output of anomaly detection. Ideally, with the percentage of outliers denoted as l, an optimal solution for $\delta(\mathbf{x}_i)$ that maximizes the objective function $J(\Theta, \Phi)$ entails setting all $\delta(\mathbf{x}_i) = 0$ for $\mathbf{x}_i$ among the l percent of outliers with lowest generation possibility $p(\mathbf{x}_i | \Theta, \Phi)$, and otherwise $\delta(\mathbf{x}_i) = 1$ is set for the remaining normal samples. Therefore, the indicator function is determined as:

$$\delta(\mathbf{x}_i) = \begin{cases} 0, & \text{if } p(\mathbf{x}_i | \Theta, \Phi) \text{ is among the } l \text{ lowest}, \\ 1, & \text{otherwise}. \end{cases} \tag{5}$$

As this method involves sorting the samples based on the generation probability as being anomalous, the values of $p(\mathbf{x}_i | \Theta, \Phi)$ can serve as a form of anomaly score, a classic approach within the mixture model framework (Reynolds et al., 2009; Zong et al., 2018). This suggests that the likelihood of a sample being anomalous is inversely related to its generative probability since a lower generative probability indicates a higher chance of the sample being an outlier. Thus the anomaly score of sample $\mathbf{x}_i$ can be defined as:

$$o_i = \frac{1}{p(\mathbf{x}_i | \Theta, \Phi)} = \frac{1}{\sum_{k=1}^{K} \omega_k \cdot \frac{\pi^{-1} \cdot |\Sigma_k|^{-1/2}}{1 + D_M(\mathbf{z}_i, \boldsymbol{\mu}_k)^2}}. \tag{6}$$

3.2. Gravity-inspired Anomaly Scoring

In practical applications, it is proved that anomaly scores derived from generation probabilities often yield suboptimal performance (Han et al., 2022). This observation prompts a reconsideration of *how to fully leverage the complex relationships among samples or even across multiple clusters for anomaly detection*. In this section, we first provide a brief introduction to the concept of Newton's Law of Universal Gravitation (Newton, 1833) and then demonstrate how the anomaly score is intriguingly similar to this cross-field principle. Finally, we discuss the advantages of introducing the vector sum operation into the anomaly score inspired by the analogy.

3.2.1. Analog Anomaly Scoring and Force Analysis

To begin with, Newton's Law of Universal Gravitation (Newton, 1833) stands as a fundamental framework for describing the interactions among entities in the physical world. According to this law, every object in the universe experiences an attractive force from another object. In classical mechanics, force analysis involves calculating the vector sum of all forces acting on an object, known as the **resultant force**, which is crucial in determining an object's acceleration or change in motion:

$$\vec{\mathbf{F}}_{i,\text{total}} = \sum_{k=1}^{K} \vec{\mathbf{F}}_{ik}, \text{ with } \vec{\mathbf{F}}_{ik} = \frac{G \cdot m_i m_k}{r_{ik}^2} \cdot \vec{\mathbf{r}}_{ik}, \tag{7}$$

where $\vec{\mathbf{F}}_{ik}$ represents the k-th force acting on the object i. This force is proportional to the product of their masses, (m_i and m_k), and inversely proportional to the square of the distance r_{ik} between them. G represents the gravitational constant, and $\vec{\mathbf{r}}_{ij}$ is the unit direction vector.

Similarly, if denoting: $\widetilde{\mathbf{F}}_{ik} = p(\mathbf{x}_i, c_i = k | \Theta, \Phi) = \omega_k \cdot \frac{\pi^{-1} \cdot |\Sigma_k|^{-1/2}}{1 + D_M(\mathbf{z}_i, \boldsymbol{\mu}_k)^2}$, the score of Equation (6) bears analogies to the summation of the magnitudes of forces as:

$$o_i = \frac{1}{\sum_{k=1}^{K} \widetilde{\mathbf{F}}_{ik}}, \text{ with } \widetilde{\mathbf{F}}_{ik} = \frac{\widetilde{G} \cdot \widetilde{m}_i \widetilde{m}_k}{\widetilde{r}_{ik}^2}, \tag{8}$$

where $\widetilde{G} = \pi^{-1}$, $\widetilde{m}_k = \omega_k |\Sigma_k|^{-1/2}$, $\widetilde{m}_i = 1$, and $\widetilde{r}_{ik} = \sqrt{1 + D_M(\mathbf{z}_i, \boldsymbol{\mu}_k)^2}$. Here, $\widetilde{r}_{ik}$ is taken as the measure of distance within the representation space, modified slightly by an additional term for smoothness. The constant $\widetilde{G}$ serves a role akin to the gravitational constant in this analogy, whereas $\widetilde{m}_k$ resembles the concept of mass for the cluster. The notation $\widetilde{m}_i$ suggests a standardization where the mass of each data point is considered uniform and not differentiated.

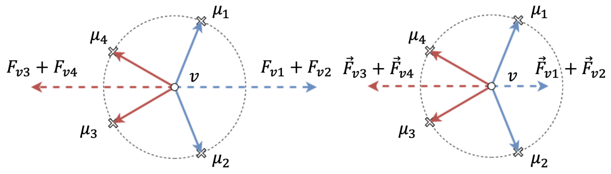

(a) Scalar Sum (b) Vector Sum

Figure 2: Analysis of gravitational force.

3.2.2. Anomaly Scoring with Vector Sum

Comparing Equation (7) with Equation (8), what still differs is that, unlike a simple sum of the scalar value, the resultant force $\vec{\mathbf{F}}_{i,\text{total}}$ employs the vector sum and incorporates both the magnitude and direction $\widehat{\mathbf{r}}_{ik}$ of each force. This distinction is crucial because forces in different directions can neutralize each other with a large angle between them or enhance each other's effects with a small angle. Inspired by this difference, we consider modeling the relationship between samples and clusters as a vector, and aggregating them through vector summation. The vector-formed anomaly score o_i^V is defined as:

$$o_i^V = \frac{1}{\| \sum_{k=1}^{K} \widetilde{\mathbf{F}}_{ik} \cdot \vec{\mathbf{r}}_{ik} \|}, \tag{9}$$

where $\vec{\mathbf{r}}_{ik}$ represents the unit direction vector in the representation space from the sample $\mathbf{z}_i$ to the cluster prototype $\boldsymbol{\mu}_k$, and $\| \cdot \|$ represents the L_2 norm.

3.2.3. Advantages of Vector Sum

The application of the vector sum principle extends beyond physical mechanics and finds relevance in various domains. In relational embedding (Bordes et al., 2013), for example, relationships can be represented as vectors. Aggregating these vectors allows for capturing complexities like transitivity, symmetry, and antisymmetry.

Similarly, in our context, the vector sum can help capture more complex relationships along clusters. In Figure 2, a sample v is attracted to two groups of cluster prototypes, $\{\boldsymbol{\mu}_1, \boldsymbol{\mu}_2\}$ and $\{\boldsymbol{\mu}_3, \boldsymbol{\mu}_4\}$, with equal mass and distances. While both groups exert equal forces, we argue that their influences differ: a sample near two clusters with a large difference is more likely to be an anomaly than one near similar clusters. For instance, a user liking both money-saving tips and luxury items is more anomalous than one liking two similar luxury items. The vector sum shows that the total force from $\{\boldsymbol{\mu}_1, \boldsymbol{\mu}_2\}$ is smaller, leading to a higher anomaly score, *thus demonstrating its effectiveness in identifying subtle distinctions among clusters*.

Algorithm 1 Model Training for UniCAD

```
Require: Data points $\mathbf{X}$, cluster number $K$, outlier ratio $l$,
    tolerance $\lambda$, iterations $t$
Ensure: Network parameters $\Theta$, mixture parameters
    $\{\omega_k, \boldsymbol{\mu}_k, \Sigma_k\}$
Initialize $\Theta$ and $\{\boldsymbol{\mu}_k, \omega_k, \Sigma_k\}$
for $i = 1$ to $t$ do
    if $i = 1$ then
        $\mathbf{X}_i \leftarrow \mathbf{X}$
    else
        Re-order points in $\mathbf{X}$ such that $o_1 \geq \cdots \geq o_n$
        $L_i \leftarrow \{x_1, \ldots, x_{\lfloor N \cdot l \rfloor}\}$
        $\mathbf{X}_i \leftarrow \mathbf{X} \setminus L_i$ {Remove top-$l$ anomalies}
    end if
    Update $\Theta$ via Equation (15)
    while $|J(\Theta, \Phi) - J^{\text{old}}(\Theta, \Phi)| > \lambda$ do
        $J^{\text{old}}(\Theta, \Phi) \leftarrow J(\Theta, \Phi)$
        Calculate $\boldsymbol{\tau}$ via Equation (10)
        Update $\{\omega_k, \boldsymbol{\mu}_k, \Sigma_k\}$ via Equations (12), (13),
        (14)
    end while
    Calculate $o_i$ via Equation (9)
end for
return $\Theta, \{\omega_k, \boldsymbol{\mu}_k, \Sigma_k\}$
```

3.3. Iterative Optimization

Given the challenge posed by the interdependence of the parameters of the network Θ and those of the mixture model $\{\omega_k, \boldsymbol{\mu}_k, \Sigma_k\}$ in joint optimization, we propose an iterative optimization procedure. The pseudocode for training the model is presented in Algorithm 1.

3.3.1. Update Φ

To update the parameters of the mixture model $\Phi = \{\omega_k, \boldsymbol{\mu}_k, \Sigma_k\}$, we use the Expectation-Maximization (EM) algorithm to maximize equation (1) (Peel & McLachlan, 2000). The detailed derivation is included in Appendix B.

E-step. During the E-step of iteration $(t+1)$, our goal is to compute the posterior probabilities of each data point belonging to the k-th cluster within the mixture model. Given the observed sample $\mathbf{x}_i$ and the current estimates of the parameters $\Theta^{(t)}$ and $\Phi^{(t)}$, the expected value of the likelihood function of latent variable c_k, or the posterior possibilities, can be expressed as:

$$\boldsymbol{\tau}_{ik}^{(t+1)} = \frac{p(\mathbf{x}_i, c_i = k | \Theta, \Phi^{(t)})}{\sum_{j=1}^{K} p(\mathbf{x}_i, c_i = j | \Theta, \Phi^{(t)})} = \frac{\widetilde{\mathbf{F}}_{ik}^{(t)}}{\sum_{j=1}^{K} \widetilde{\mathbf{F}}_{ij}^{(t)}}. \tag{10}$$

The scale factor(Peel & McLachlan, 2000) serving as an intermediate result for subsequent updates in the M-step is :

$$\mathbf{u}_{ik}^{(t+1)} = \frac{2}{1 + D_M(\mathbf{z}_i^{(t)}, \boldsymbol{\mu}_k^{(t)})}. \tag{11}$$

M-step. In the M-step of iteration $(t+1)$, given the gradients $\frac{\partial J(\Theta,\Phi)}{\partial \omega_k} = 0$, $\frac{\partial J(\Theta,\Phi)}{\partial \boldsymbol{\mu}_k} = 0$, and $\frac{\partial J(\Theta,\Phi)}{\partial \Sigma_k} = 0$, we derive the analytical solutions for the mixture model parameters ω_k, $\boldsymbol{\mu}_k$, and Σ_k. Assume the anomalous ratio is $l \in [0, 1]$, the number of the normal samples is $n = \text{int}(l * N)$. The updating process for $\{\omega_k^{(t+1)}, \boldsymbol{\mu}_k^{(t+1)}, \boldsymbol{\Sigma}_k^{(t+1)}\}$ is as follows:

- The mixture weights ω_k are updated by averaging the posterior probabilities over all data points with the number of samples , reflecting the relative presence of each component in the mixture:

$$\omega_k^{(t+1)} = \sum_{i=1}^{n} \boldsymbol{\tau}_{ik}^{(t+1)} / n. \tag{12}$$

- The prototypes $\boldsymbol{\mu}_k$ are updated to be the weighted average of the data points, where weights are the posterior probabilities:

$$\boldsymbol{\mu}_k^{(t+1)} = \sum_{i=1}^{n} \left(\boldsymbol{\tau}_{ik}^{(t+1)} \mathbf{u}_{ik}^{(t+1)} \mathbf{z}_i \right) / \sum_{i=1}^{n} \left(\boldsymbol{\tau}_{ik}^{(t+1)} \mathbf{u}_{ik}^{(t+1)} \right). \tag{13}$$

- The covariance matrices Σ_k are updated by considering the dispersion of the data around the newly computed prototypes:

$$\boldsymbol{\Sigma}_k^{(t+1)} = \frac{\sum_{i=1}^{n} \boldsymbol{\tau}_{ik}^{(t+1)} \mathbf{u}_{ik}^{(t+1)} (\mathbf{z}_i - \boldsymbol{\mu}_k^{(t+1)})(\mathbf{z}_i - \boldsymbol{\mu}_k^{(t+1)})^{\intercal}}{\sum_{j=1}^{K} \boldsymbol{\tau}_{ij}^{(t+1)}}. \tag{14}$$

3.3.2. Update Θ

We focus on anomaly-aware representation learning and use stochastic gradient descent to optimize the network parameters Θ, by minimizing the following joint loss:

$$\mathcal{L} = -J(\Theta, \Phi) + g(\Theta), \tag{15}$$

where $J(\Theta, \Phi) = \log p(\mathbf{X}|\Theta, \Phi)$. An additional constraint term $g(\Theta)$ is introduced to prevent shortcut solution (Geirhos et al., 2020). In practice, an autoencoder architecture is implemented, utilizing a reconstruction loss $g(\Theta) = \|x - \hat{x}\|^2$ as the constraint.

These updates are iteratively performed until convergence, resulting in optimized model parameters that best fit the given data according to the mixture model framework.

4. Experiments

4.1. Datasets & Baselines

We evaluated UniCAD on an extensive collection of datasets, comprising 30 tabular datasets that span 16 diverse fields. We specifically focused on naturally occurring anomaly patterns, rather than synthetically generated or injected anomalies, as this aligns more closely with real-world scenarios. The detailed descriptions are provided in Table 4 of Appendix D.1. Following the setup in ADBench (Han et al., 2022), we adopt an inductive setting to predict newly emerging data, a highly beneficial approach for practical applications. The code for reproducing our experiments is publicly available at `https://github.com/BabelTower/UniCAD`.

To assess the effectiveness of UniCAD, we compared it with 17 advanced unsupervised anomaly detection methods, including: (1) *traditional methods*: SOD (Kriegel et al., 2009) and HBOS (Goldstein & Dengel, 2012); (2) *linear methods*: PCA (Wold et al., 1987) and OCSVM (Manevitz & Yousef, 2001); (3) *density-based methods*: LOF (Breunig et al., 2000) and KNN (Peterson, 2009); (4) *ensemble-based methods*: LODA (Pevnỳ, 2016) and IForest (Liu et al., 2008); (5) *probability-based methods*: DAGMM (Zong et al., 2018), ECOD (Li et al., 2022), and COPOD (Li et al., 2020); (6) *cluster-based methods*: DBSCAN (Ester et al., 1996), CBLOF (He et al., 2003), DCOD (Song et al., 2021) and KMeans-- (Chawla & Gionis, 2013); and (7) *representation-based methods*: DeepSVDD (Ruff et al., 2018) and DIF (Xu et al., 2023). These baselines encompass the majority of the latest methods, providing a comprehensive overview of the state-of-the-art. For a detailed description, please refer to Appendix D.2.

4.2. Experiment Settings

In the unsupervised setting, we employ the default hyperparameters from the original papers for all comparison methods. Similarly, the UniCAD also utilizes a fixed set of parameters to ensure a fair comparison. For all datasets, we employ a two-layer MLP with a hidden dimension of $d = 128$ and ReLU activation function as both encoder and decoder. We utilize the Adam optimizer (Kingma & Ba, 2014) with a learning rate of $1e^{-4}$ for 100 epochs. For the EM process, we set the maximum iteration number to 100 and a tolerance of $1e^{-3}$ for stopping training when the objectives converge. The number of components in the mixture model is set as $k = 10$, and the proportion of the outlier is set as $l = 1\%$. We evaluate the methods using Area Under the Receiver Operating Characteristic (AUC-ROC) and Area Under the Precision-Recall Curve (AUC-PR) metrics (Han et al., 2022), reporting the average ranking (Avg. Rank) across all datasets. All experiments are run 3 times with different seeds, and the mean results are reported.

Table 1: AUCROC of 10 unsupervised algorithms on 30 tabular benchmark datasets. In each dataset, the algorithm with the highest AUCROC is marked in red, the second highest in blue, and the third highest in green.

Dataset	OC SVM	LOF	IForest	DA GMM	ECOD	DB SCAN	CBLOF	DCOD	KMeans--	DIF	UniCAD w/ o_i^S	UniCAD w/ o_i^V
annthyroid	57.23	70.20	82.01	56.53	78.66	50.08	62.28	55.01	64.99	66.76	75.27	72.72
backdoor	85.04	85.79	72.15	55.98	86.08	76.55	81.91	79.57	89.11	92.87	87.28	89.24
breastw	80.30	40.61	98.32	N/A	99.17	85.20	96.86	99.02	97.05	77.45	98.15	98.56
campaign	65.70	59.04	71.71	56.03	76.10	50.60	64.34	63.16	63.51	67.53	73.52	73.64
celeba	70.70	38.95	70.41	44.74	76.48	50.36	73.99	91.41	56.76	65.29	81.38	82.00
census	54.90	47.46	59.52	59.65	67.63	58.50	60.17	72.84	63.33	59.66	67.90	67.84
glass	35.36	69.20	77.13	76.09	65.83	54.55	78.30	78.07	77.30	84.57	79.52	82.17
Hepatitis	67.75	38.06	69.75	54.80	75.22	68.12	73.05	48.38	64.64	74.24	75.53	80.62
http	99.59	27.46	99.96	N/A	98.10	49.97	99.60	99.53	99.55	99.49	99.53	99.52
Ionosphere	75.92	90.59	84.50	73.41	73.15	81.12	90.79	57.78	91.36	89.74	92.04	90.37
landsat	36.15	53.90	47.64	43.92	36.10	50.17	63.69	33.40	55.31	54.84	49.60	57.37
Lymphography	99.54	89.86	99.81	72.11	99.52	74.16	99.81	81.19	100.00	83.67	99.29	99.73
mnist	82.95	67.13	80.98	67.23	74.61	50.00	79.96	65.23	82.45	88.16	86.00	86.64
musk	80.58	41.18	99.99	76.85	95.40	50.00	100.00	42.19	72.16	98.22	99.92	100.00
pendigits	93.75	47.99	94.76	64.22	93.01	55.33	96.93	94.33	94.37	93.79	95.12	95.52
Pima	66.92	65.71	72.87	55.93	63.05	51.39	71.49	72.16	70.44	67.28	75.16	74.87
satellite	59.02	55.88	70.43	62.33	58.09	55.52	71.32	55.97	67.71	74.52	72.46	77.65
satimage-2	97.35	47.36	99.16	96.29	96.28	75.74	99.84	86.01	99.88	99.63	99.87	99.88
shuttle	97.40	57.11	99.56	97.92	99.13	50.40	93.07	97.20	69.97	97.00	99.15	98.75
skin	49.45	46.47	68.21	N/A	49.08	50.00	68.03	64.34	65.47	66.36	72.26	69.69
Stamps	83.86	51.26	91.21	88.89	87.87	52.08	69.89	93.41	79.78	87.95	91.37	94.18
thyroid	87.92	86.86	98.30	79.75	97.94	53.57	94.74	78.55	92.26	96.26	97.66	97.48
vertebral	37.99	49.29	36.66	53.20	40.66	49.74	41.01	38.13	38.14	47.20	33.11	47.37
vowels	61.59	93.12	73.94	60.58	62.24	57.50	92.12	51.56	93.45	81.02	88.38	92.09
Waveform	56.29	73.32	71.47	49.35	62.36	66.41	71.27	63.47	74.35	75.33	71.81	74.29
WBC	99.03	54.17	99.01	N/A	99.11	87.43	96.88	94.92	97.45	81.27	97.68	98.93
Wilt	31.28	50.65	41.94	37.29	36.30	49.96	34.50	44.71	34.91	39.46	48.95	52.56
wine	73.07	37.74	80.37	61.70	77.22	40.33	27.14	82.18	27.36	41.69	82.72	95.25
WPBC	45.35	41.41	46.63	47.80	46.65	52.22	45.32	49.67	45.01	44.69	48.02	49.90
Avg. Rank	**7.8**	**8.9**	**5.1**	**8.7**	**6.4**	**9.3**	**5.7**	**7.4**	**6.0**	**5.8**	**3.7**	**2.6**

4.3. Performance and Analysis

Performance Comparison. Table 1 presents a comparison of UniCAD with 10 unsupervised baseline methods across 30 tabular datasets using the AUC-ROC metric. The experimental results, which encompass 17 baselines, are included in Tables 5 and 6 of Appendix D.3. Our proposed UniCAD achieves the top average ranking, exhibiting the best or near-best performance on a larger number of datasets and confirming advanced capabilities. It is noteworthy that there is no one-size-fits-all unsupervised anomaly detection method suitable for every type of dataset, as demonstrated by the observation that other methods have also achieved some of the best results on certain datasets. However, our model showcased a remarkable ability to generalize across most datasets featuring natural anomalies, as evidenced by statistical average ranking. As for clustering-based methods such as KMeans--, DCOD, and CBLOF, they mostly rank in the top tier among all baseline methods, supporting the advantage of combining deep clustering with anomaly detection. However, our method significantly outperformed these methods by mitigating their limitations and further providing a unified framework for joint representation learning, clustering, and anomaly detection.

Effectiveness of Vector Sum in Anomaly Scoring. As demonstrated in Table 1, we compare the anomaly score $\mathbf{o}_i$ derived directly from the generation possibility with its vector summation form $\mathbf{o}_i^V$. According to our statistical findings, we observe that vector scores $\mathbf{o}_i^V$ consistently outperform scalar scores $\mathbf{o}_i$. This indicates that the introduction of the vector summation, analogous to the concept of resultant force, makes a substantial difference in anomaly detection scenarios involving multiple clusters. The performance gains of the vector sum scores strongly demonstrate the effectiveness of the UniCAD in capturing the subtle differences in the distinctions among multiple clusters and underscore the utility of this factor in the context of anomaly detection based on clustering.

Runtime Comparison. We present a analysis of the runtime performance of various methods, including our proposed approach, as detailed in Table 2. Our experiments, conducted on the backdoor dataset, reveal that while non-

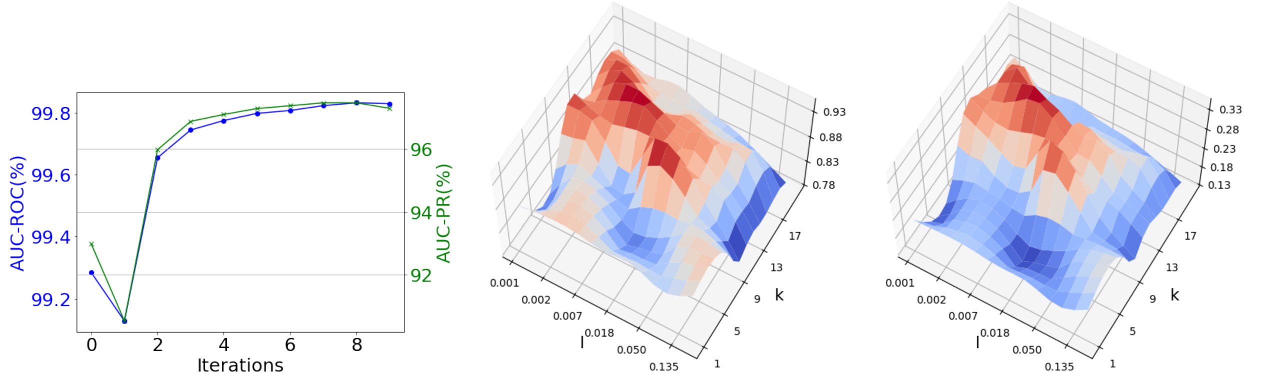

(a) Optimization Analysis

(b) AUC-ROC Surface

(c) AUC-PR Surface

Figure 3: (a) demonstrates the performance variations during the optimization process on the satimage-2 dataset. (b) & (c) Analysis of cluster count k, anomaly ratio l.

Table 2: Runtime Comparison. The runtime is reported in seconds (s).

Phase	IForest	KMeans--	DAGMM	DCOD	UniCAD
Fit	0.256	103.697	795.004	4548.634	246.113
Infer	0.018	0.059	4.190	16.190	0.079

Table 3: Ablation Study on 30 Datasets (AUC-ROC)

Metric	Gauss. Dist.	w/o Objective	w/o Indicator	Full Model
Avg. Rank	6.2	6.6	5.0	**4.2**

deep learning methods exhibit lower runtime, they often simplify the problem space excessively, failing to capture the complex non-linear relationships present in the data. In contrast, our method, when compared to existing deep learning techniques, demonstrates a significant reduction in computational time. This indicates that our approach not only manages to efficiently model complex patterns but also achieves an optimal balance between computational efficiency and modeling capability.

4.4. Ablation Studies

In this section, we examine the contributions of different components in UniCAD. Tables 3 reports the results. We make three major observations. **Firstly**, the anomaly detection performance experiences a significant drop when replacing the Student's t distribution with a Gaussian distribution for the Mixture Model, highlighting the robustness of the Student's t distribution in unsupervised anomaly detection. **Secondly**, omitting the likelihood maximization loss (w/o $J(\Theta, \Phi)$) also results in a considerable decrease in overall performance. This observation underscores the importance of deriving both the optimization objectives and anomaly scores from the likelihood generation probability through a theoretical framework, which allows for unified joint optimization of anomaly detection and clustering in the representation space. **Furthermore**, the indicator function $\delta(\mathbf{x}_i)$ also contributes to a performance increase. These results further confirm the effectiveness of our UniCAD in mitigating the negative influence of anomalies in the clustering process, as the existence of outliers may significantly degrade the performance of clustering. In summary, all these ablation studies clearly demonstrate the effectiveness of our theoretical framework in simultaneously considering representation learning, clustering, and anomaly detection.

4.5. Hyperparameters Analysis

This section analyzes how hyperparameters affect our model's performance during the iterative training process. As shown in Figure 3a, we tracked iteration counts from 0 to 10 for the satimage-2 dataset, keeping other parameters constant. The AUC-ROC and AUC-PR curves demonstrated stable performance with only minor fluctuations initially, highlighting the convergence of the iterative EM optimization. We also conducted a sensitivity analysis on key hyperparameters for the donors dataset, focusing on the number of clusters k and the outlier set proportion l. The results, shown in Figure 3, reveal that the optimal l is generally lower than the actual anomaly proportion. Furthermore, a pattern was observed with the number of clusters k, where the model performance initially improved with an increase in k, followed by a subsequent decline. This suggests the existence of an optimal range for the number of clusters, which should be carefully selected based on the specific application context.

5. Conclusion

This paper presents UniCAD, a novel model for Unsupervised Anomaly Detection (UAD) that seamlessly integrates representation learning, clustering, and anomaly detection within a unified theoretical framework. Specifically, UniCAD introduces an anomaly-aware data likelihood based on the mixture model with the Student-t distribution to guide the joint optimization process, effectively mitigating the impact of anomalies on representation learning and clustering. This framework enables a theoretically grounded anomaly score inspired by universal gravitation, which considers complex relationships between samples and multiple clusters. Extensive experiments on 30 datasets across various domains demonstrate the effectiveness and generalization capability of UniCAD, surpassing 15 baseline methods and establishing it as a state-of-the-art solution in unsupervised anomaly detection.

Impact Statement

This paper presents work whose goal is to advance the field of Machine Learning. There are many potential societal consequences of our work, none which we feel must be specifically highlighted here.

Acknowledgements

This work is supported by the National Natural Science Foundation of China (Grant No. 62476245), Zhejiang Provincial Natural Science Foundation of China (Grant No. LTGG23F030005).

References

Andrade, J. A. A. On the robustness to outliers of the student-t process. *Scandinavian Journal of Statistics*, 50 (2):725–749, 2023.

Aytekin, C., Ni, X., Cricri, F., and Aksu, E. Clustering and unsupervised anomaly detection with l 2 normalized deep auto-encoder representations. In *2018 International Joint Conference on Neural Networks (IJCNN)*, pp. 1–6. IEEE, 2018.

Bakumenko, A. and Elragal, A. Detecting anomalies in financial data using machine learning algorithms. *Systems*, 10(5):130, 2022.

Bordes, A., Usunier, N., Garcia-Duran, A., Weston, J., and Yakhnenko, O. Translating embeddings for modeling multi-relational data. *Advances in neural information processing systems*, 26, 2013.

Breunig, M. M., Kriegel, H.-P., Ng, R. T., and Sander, J. Lof: identifying density-based local outliers. In *Proceedings of the 2000 ACM SIGMOD international conference on Management of data*, pp. 93–104, 2000.

Chalapathy, R. and Chawla, S. Deep learning for anomaly detection: A survey. *arXiv preprint arXiv:1901.03407*, 2019.

Chandola, V., Banerjee, A., and Kumar, V. Anomaly detection: A survey. *ACM computing surveys (CSUR)*, 41(3): 1–58, 2009.

Chawla, S. and Gionis, A. k-means–: A unified approach to clustering and outlier detection. In *Proceedings of the 2013 SIAM international conference on data mining*, pp. 189–197. SIAM, 2013.

Cho, H., Seol, J., and Lee, S.-g. Masked contrastive learning for anomaly detection. *arXiv preprint arXiv:2105.08793*, 2021.

Duan, L., Xu, L., Liu, Y., and Lee, J. Cluster-based outlier detection. *Annals of Operations Research*, 168:151–168, 2009.

Ester, M., Kriegel, H.-P., Sander, J., Xu, X., et al. A density-based algorithm for discovering clusters in large spatial databases with noise. In *kdd*, volume 96, pp. 226–231, 1996.

Geirhos, R., Jacobsen, J.-H., Michaelis, C., Zemel, R., Brendel, W., Bethge, M., and Wichmann, F. A. Shortcut learning in deep neural networks. *Nature Machine Intelligence*, 2(11):665–673, 2020.

Goldstein, M. and Dengel, A. Histogram-based outlier score (hbos): A fast unsupervised anomaly detection algorithm. *KI-2012: poster and demo track*, 1:59–63, 2012.

Goyal, S., Raghunathan, A., Jain, M., Simhadri, H. V., and Jain, P. Drocc: Deep robust one-class classification. In *International conference on machine learning*, pp. 3711–3721. PMLR, 2020.

Han, S., Hu, X., Huang, H., Jiang, M., and Zhao, Y. Adbench: Anomaly detection benchmark. *Advances in Neural Information Processing Systems*, 35:32142–32159, 2022.

He, Z., Xu, X., and Deng, S. Discovering cluster-based local outliers. *Pattern recognition letters*, 24(9-10):1641–1650, 2003.

Kingma, D. P. and Ba, J. Adam: A method for stochastic optimization. *arXiv preprint arXiv:1412.6980*, 2014.

Kou, Y., Lu, C.-T., Sirwongwattana, S., and Huang, Y.-P. Survey of fraud detection techniques. In *IEEE International Conference on Networking, Sensing and Control, 2004*, volume 2, pp. 749–754. IEEE, 2004.

Kriegel, H.-P., Kröger, P., Schubert, E., and Zimek, A. Outlier detection in axis-parallel subspaces of high dimensional data. In *Advances in Knowledge Discovery and Data Mining: 13th Pacific-Asia Conference, PAKDD 2009 Bangkok, Thailand, April 27-30, 2009 Proceedings 13*, pp. 831–838. Springer, 2009.

Li, J., Izakian, H., Pedrycz, W., and Jamal, I. Clustering-based anomaly detection in multivariate time series data. *Applied Soft Computing*, 100:106919, 2021.

Li, Z., Zhao, Y., Botta, N., Ionescu, C., and Hu, X. Copod: copula-based outlier detection. In *2020 IEEE international conference on data mining (ICDM)*, pp. 1118–1123. IEEE, 2020.

Li, Z., Zhao, Y., Hu, X., Botta, N., Ionescu, C., and Chen, G. Ecod: Unsupervised outlier detection using empirical cumulative distribution functions. *IEEE Transactions on Knowledge and Data Engineering*, 2022.

Liu, F. T., Ting, K. M., and Zhou, Z.-H. Isolation forest. In *2008 eighth ieee international conference on data mining*, pp. 413–422. IEEE, 2008.

Manevitz, L. M. and Yousef, M. One-class svms for document classification. *Journal of machine Learning research*, 2(Dec):139–154, 2001.

McLachlan, G. J. Mahalanobis distance. *Resonance*, 4(6): 20–26, 1999.

Newton, I. *Philosophiae naturalis principia mathematica*, volume 1. G. Brookman, 1833.

Peel, D. and McLachlan, G. J. Robust mixture modelling using the t distribution. *Statistics and computing*, 10: 339–348, 2000.

Peterson, L. E. K-nearest neighbor. *Scholarpedia*, 4(2): 1883, 2009.

Pevnỳ, T. Loda: Lightweight on-line detector of anomalies. *Machine Learning*, 102:275–304, 2016.

Qiu, C., Pfrommer, T., Kloft, M., Mandt, S., and Rudolph, M. Neural transformation learning for deep anomaly detection beyond images. In *International conference on machine learning*, pp. 8703–8714. PMLR, 2021.

Reynolds, D. A. et al. Gaussian mixture models. *Encyclopedia of biometrics*, 741(659-663), 2009.

Ruff, L., Vandermeulen, R., Goernitz, N., Deecke, L., Siddiqui, S. A., Binder, A., Müller, E., and Kloft, M. Deep one-class classification. In *International conference on machine learning*, pp. 4393–4402. PMLR, 2018.

Ruff, L., Kauffmann, J. R., Vandermeulen, R. A., Montavon, G., Samek, W., Kloft, M., Dietterich, T. G., and Müller, K.-R. A unifying review of deep and shallow anomaly detection. *Proceedings of the IEEE*, 109(5):756–795, 2021.

Salem, O., Liu, Y., Mehaoua, A., and Boutaba, R. Online anomaly detection in wireless body area networks for reliable healthcare monitoring. *IEEE journal of biomedical and health informatics*, 18(5):1541–1551, 2014.

Song, H., Li, P., and Liu, H. Deep clustering based fair outlier detection. In *Proceedings of the 27th ACM SIGKDD Conference on Knowledge Discovery & Data Mining*, pp. 1481–1489, 2021.

Van Der Maaten, L. Learning a parametric embedding by preserving local structure. In *Artificial intelligence and statistics*, pp. 384–391. PMLR, 2009.

Wold, S., Esbensen, K., and Geladi, P. Principal component analysis. *Chemometrics and intelligent laboratory systems*, 2(1-3):37–52, 1987.

Xie, J., Girshick, R., and Farhadi, A. Unsupervised deep embedding for clustering analysis. In *International conference on machine learning*, pp. 478–487. PMLR, 2016.

Xu, H., Pang, G., Wang, Y., and Wang, Y. Deep isolation forest for anomaly detection. *IEEE Transactions on Knowledge and Data Engineering*, 2023.

Zhou, S., Huang, X., Liu, N., Tan, Q., and Chung, F.-L. Unseen anomaly detection on networks via multi-hypersphere learning. In *Proceedings of the 2022 SIAM International Conference on Data Mining (SDM)*, pp. 262–270. SIAM, 2022.

Zong, B., Song, Q., Min, M. R., Cheng, W., Lumezanu, C., Cho, D., and Chen, H. Deep autoencoding gaussian mixture model for unsupervised anomaly detection. In *International conference on learning representations*, 2018.

A. Iterative Training Algorithm

B. Derivation of EM Algorithm

This appendix provides the detailed derivation of the Expectation-Maximization (EM) algorithm for optimizing the parameters of a mixture model based on Student's t-distribution. The focus is on deriving analytical solutions for the maximization of the parameters $\Phi = \{\boldsymbol{\mu}_k, \Sigma_k, \omega_k\}$ of the mixture components. The EM algorithm alternates between two steps:

In the E-step, we calculate the posterior probabilities $\boldsymbol{\tau}_{ik}$, representing the probability of data point i belonging to cluster k, given the current parameters. The posterior probabilities for a Student's t-distribution mixture model are formulated as:

$$\boldsymbol{\tau}_{ik} = \frac{\omega_k \cdot p(\mathbf{z}_i|\boldsymbol{\mu}_k, \Sigma_k)}{\sum_{j=1}^{K} \omega_j \cdot p(\mathbf{z}_i|\boldsymbol{\mu}_j, \Sigma_j)}, \tag{16}$$

where $\boldsymbol{\tau}(\mathbf{z}_i|\boldsymbol{\mu}_k, \Sigma_k)$ denotes the Student's t-distribution for data point i with respect to cluster k, and K is the number of mixture components.

The Student's t-distribution is depicted as a hierarchical conditional probability, resembling a Gaussian distribution with an accuracy scale factor $\mathbf{u}$, where its latent variable follows a gamma distribution. Adopting a degree of freedom $\nu = 1$, the value of $\mathbf{u}_{ik}$ is given by:

$$\mathbf{u}_{ik} = \frac{\nu + 1}{\nu + D_M(z_i, \boldsymbol{\mu}_k)} = \frac{2}{1 + D_M(z_i, \boldsymbol{\mu}_k)} \tag{17}$$

In the M-step, we update the parameters $\Phi = \{\omega_k, \boldsymbol{\mu}_k, \text{and } \Sigma_k\}$ using the derivatives obtained in the previous steps. In our model, the likelihood function for a Student's-t Distribution Mixture Model (SMM) is represented as:

$$L(\omega, \boldsymbol{\mu}, \Sigma) = \sum_{i=1}^{N} \sum_{k=1}^{K} \omega_k \cdot \frac{\pi^{-1} \cdot |\Sigma_k|^{-\frac{1}{2}}}{1 + (\mathbf{z}_i - \boldsymbol{\mu}_k)^T \Sigma_k^{-1} (\mathbf{z}_i - \boldsymbol{\mu}_k)}, \tag{18}$$

where ω_k are the mixture weights, Σ_k the covariance matrices, $\boldsymbol{\mu}_k$ the means, and $\mathbf{z}_i$ the data points.

The derivative with respect to ω_k must consider the constraint that the sum of the mixture weights equals 1, i.e., $\sum_k \omega_k = 1$. Hence, we introduce a Lagrange multiplier λ to address this constraint and construct the Lagrangian L':

$$L'(\omega, \boldsymbol{\mu}, \Sigma, \lambda) = L(\omega, \boldsymbol{\mu}, \Sigma) + \lambda \left(1 - \sum_{k=1}^{K} \omega_k \right), \tag{19}$$

The derivative with respect to ω_k is:

$$\frac{\partial L'}{\partial \omega_k} = \frac{\partial L}{\partial \omega_k} - \lambda, \tag{20}$$

Substituting the definition of $L(\omega, \boldsymbol{\mu}, \Sigma)$, we obtain:

$$\frac{\partial L}{\partial \omega_k} = \sum_i \frac{p(\mathbf{z}_i|\boldsymbol{\mu}_k, \Sigma_k)}{\sum_{j=1}^{K} \omega_j \cdot p(\mathbf{z}_i|\boldsymbol{\mu}_j, \Sigma_j)} = \sum_i \frac{\boldsymbol{\tau}_{ik}}{\omega_k}, \tag{21}$$

To solve for ω_k, we first multiply both sides of the equation by ω_k and apply the constraint condition:

$$\sum_k \omega_k \left(\sum_i \frac{\boldsymbol{\tau}_{ik}}{\omega_k} - \lambda \right) = 0, \tag{22}$$

Upon further organization, we find that the Lagrange multiplier λ actually equals the total number of data points N (since $\sum_i \boldsymbol{\tau}_{ik} = N_k$, where N_k is the expected total number of data points belonging to the kth component, and the sum of all N_k equals the total number of data points N).

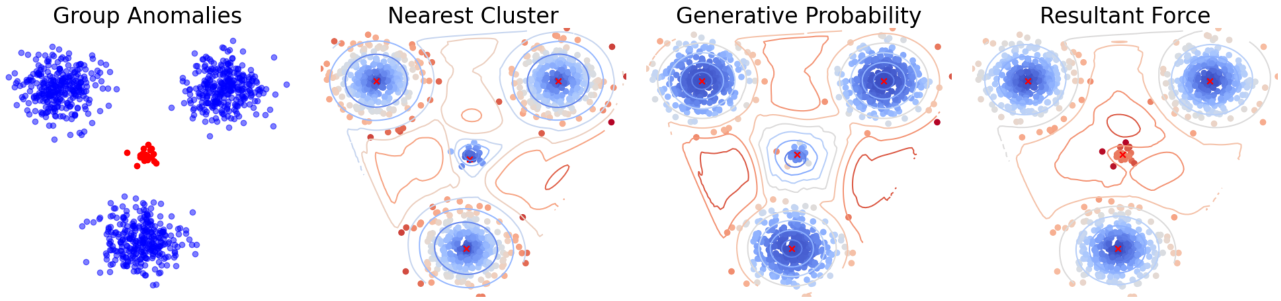

Figure 4: Score comparison with other methods.

Finally, we can solve for ω_k:

$$\omega_k = \frac{\sum_i \boldsymbol{\tau}_{ik}}{N}, \tag{23}$$

This result indicates that the weight ω_k of each mixture component equals the proportion of the posterior probabilities of the data points it contains relative to all data points.

To update $\boldsymbol{\mu}_k$ and Σ_k, we consider the conditional expectation of the data log-likelihood function:

$$\begin{aligned} Q(\boldsymbol{\mu}_k, \Sigma_k) = \sum_{i=1}^{N} \boldsymbol{\tau}_{ik} \Big(&- \log(\pi) - \frac{1}{2}\log|\sigma_k| + \frac{1}{2}\log u_{ik} \\ &- \frac{1}{2}\mathbf{u}_{ik}(\mathbf{z}_i - \boldsymbol{\mu}_k)^T \Sigma_k^{-1} (\mathbf{z}_i - \boldsymbol{\mu}_k) \Big) \end{aligned} \tag{24}$$

Maximizing $Q(\boldsymbol{\mu}_k, \Sigma_k)$ with respect to $\boldsymbol{\mu}_k$ leads to:

$$\frac{\partial Q}{\partial \boldsymbol{\mu}_k} = \frac{1}{2}\sum_{i=1}^{N} \boldsymbol{\tau}_{ik}\mathbf{u}_{ik}(2\Sigma_k^{-1}\boldsymbol{\mu}_k - 2\Sigma_k^{-1}\mathbf{z}_{ik}) \tag{25}$$

Setting $\frac{\partial Q}{\partial \boldsymbol{\mu}_k} = 0$ results in the updated mean $\boldsymbol{\mu}_k^{(t+1)}$:

$$\boldsymbol{\mu}_k^{(t+1)} = \sum_{i=1}^{n} \left(\boldsymbol{\tau}_{ik}^{(t+1)} \mathbf{u}_{ik}^{(t+1)} \mathbf{z}_i \right) / \sum_{i=1}^{n} \left(\boldsymbol{\tau}_{ik}^{(t+1)} \mathbf{u}_{ik}^{(t+1)} \right). \tag{26}$$

Considering the derivative of $Q(\boldsymbol{\mu}_k, \Sigma_k)$ with respect to Σ_k^{-1}:

$$\frac{\partial Q}{\partial \Sigma_k^{-1}} = \frac{1}{2}\sum_{i=1}^{N} \boldsymbol{\tau}_{ik} \left(\Sigma_k - \mathbf{u}_{ik}(\mathbf{z}_i - \boldsymbol{\mu}_k) \times (\mathbf{z}_i - \boldsymbol{\mu}_k)^T \right). \tag{27}$$

Setting $\frac{\partial Q}{\partial \boldsymbol{\mu}_k} = 0$ yields the updated covariance matrix $\boldsymbol{\Sigma}_k^{(t+1)}$:

$$\boldsymbol{\Sigma}_k^{(t+1)} = \frac{\sum_{i=1}^{n} \boldsymbol{\tau}_{ik}^{(t+1)} \mathbf{u}_{ik}^{(t+1)} (\mathbf{z}_i - \boldsymbol{\mu}_k^{(t+1)})(\mathbf{z}_i - \boldsymbol{\mu}_k^{(t+1)})^T}{\sum_{j=1}^{K} \boldsymbol{\tau}_{ij}^{(t+1)}}. \tag{28}$$

C. Anomaly Score with Vector Sum

C.1. Toy Example

In the appendix, as illustrated in Figure 4, we investigated a toy example. We discussed a specific pattern of anomalies termed *group anomalies*, where a small number of anomalous samples cluster together. It is crucial to note that we do not claim this anomaly pattern is common in real-world data; our goal is merely to point out a specific anomaly pattern that is challenging for traditional cluster-based anomaly detection methods to detect. Specifically, we utilize three Gaussian distributions with high variance (each generating 300 data samples) and one with lower variance (generating 30 data samples). Because the samples from the smaller Gaussian follow a different generative mechanism and represent a minority in the dataset, we consider them anomalies.

We set the cluster number for KMeans-- and GMM at four, indicating that the Gaussian distribution comprising anomalous samples was also recognized as a cluster. KMeans-- employs a cluster-based approach, using the distance to the nearest cluster center as the anomaly score, while GMM uses a probability-based approach, considering the samples' likelihood in the mixture model as the anomaly score. However, both approaches are ineffective in this scenario. Rather than identifying the small cluster as anomalous, they tend to misidentify samples on the peripheries of larger clusters as anomalies.

By contrast, our scoring method views the entire small cluster as more likely anomalous, followed by outlier samples on the margins of the larger clusters. This visualization provides a perspective that distinguishes our method from previous efforts.

D. Experimental Supplementary

D.1. Benchmark Datasets Details

Due to space constraints in the main text, we utilized 30 public datasets from ADBench (Han et al., 2022), covering all different types of data. The details of the 30 datasets are presented in Table 4.

D.2. Baselines Details

A comprehensive overview of the unsupervised anomaly detection methods is presented below.

D.2.1. Traditional Models

- **Subspace Outlier Detection (SOD) (Kriegel et al., 2009):** Identifies outliers in varying subspaces of a high-dimensional feature space, targeting anomalies that emerge in lower-dimensional projections.

- **Histogram-based Outlier Detection (HBOS) (Goldstein & Dengel, 2012):** Assumes feature independence and calculates outlyingness via histograms, offering scalability and efficiency.

D.2.2. Linear Models

- **Principal Component Analysis (PCA) (Wold et al., 1987):** Utilizes singular value decomposition for dimensionality reduction, with anomalies indicated by reconstruction errors.

- **One-class SVM (OCSVM) (Manevitz & Yousef, 2001):** Defines a decision boundary to separate normal samples from outliers, maximizing the margin from the data origin.

D.2.3. Density-based Models

- **Local Outlier Factor (LOF) (Breunig et al., 2000) :** Measures local density deviation, marking samples as outliers if they lie in less dense regions compared to their neighbors.

- **K-Nearest Neighbors (KNN) (Peterson, 2009):** Anomaly scores are assigned based on the distance to the k-th nearest neighbor, embodying a simple yet effective approach.

D.2.4. Ensemble-based Models

- **Lightweight On-line Detector of Anomalies (LODA) (Pevnỳ, 2016) :** An ensemble method suitable for real-time processing and adaptable to concept drift through random projections and histograms.

- **Isolation Forest (IForest) (Liu et al., 2008):** Isolates anomalies by randomly selecting features and split values, leveraging the ease of isolating anomalies to identify them efficiently.

Table 4: Statistics of tabular benchmark datasets.

Data	# Samples	# Features	# Anomaly	% Anomaly	Category
annthyroid	7200	6	534	7.42	Healthcare
backdoor	95329	196	2329	2.44	Network
breastw	683	9	239	34.99	Healthcare
campaign	41188	62	4640	11.27	Finance
celeba	202599	39	4547	2.24	Image
census	299285	500	18568	6.20	Sociology
glass	214	7	9	4.21	Forensic
Hepaitis	80	19	13	16.25	Healthcare
http	567498	3	2211	0.39	Web
Ionosphere	351	33	126	35.90	Oryctognosy
landsat	6435	36	1333	20.71	Astronautics
Lymphography	148	18	6	4.05	Healthcare
magic.gamma	19020	10	6688	35.16	Physical
mnist	7603	100	700	9.21	Image
musk	3062	166	97	3.17	Chemistry
pendigits	6870	16	156	2.27	Image
Pima	768	8	268	34.90	Healthcare
satellite	6435	36	2036	31.64	Astronautics
satimage-2	5803	36	71	1.22	Astronautics
shuttle	49097	9	3511	7.15	Astronautics
skin	245057	3	50859	20.75	Image
Stamps	340	9	31	9.12	Document
thyroid	3772	6	93	2.47	Healthcare
vertebral	240	6	30	12.50	Biology
vowels	1456	12	50	3.43	Linguistics
Waveform	3443	21	100	2.90	Physics
WBC	223	9	10	4. 48	Healthcare
Wilt	4819	5	257	5.33	Botany
wine	129	13	10	7.75	Chemistry
WPBC	198	33	47	23.74	Healthcare

D.2.5. Probability-based Models

- **Deep Autoencoding Gaussian Mixture Model (DAGMM) (Zong et al., 2018):** Combines a deep autoencoder with a GMM for anomaly scoring, utilizing both low-dimensional representation and reconstruction error.

- **Empirical-Cumulative-distribution-based Outlier Detection (ECOD) (Li et al., 2022):** Uses ECDFs to estimate feature densities independently, targeting outliers in distribution tails.

- **Copula Based Outlier Detector (COPOD) (Li et al., 2020):** A hyperparameter-free method leveraging empirical copula models for interpretable and efficient outlier detection.

D.2.6. Cluster-based Models

- **DBSCAN (Ester et al., 1996):** A density-based clustering algorithm that identifies clusters based on the density of data points, effectively separating high-density clusters from low-density noise, and is widely used for anomaly detection in spatial data.

- **Clustering Based Local Outlier Factor (CBLOF) (He et al., 2003):** Calculates anomaly scores based on cluster distances, using global data distribution.

- **KMeans-- (Song et al., 2021):** Extends k-means to include outlier detection in the clustering process, offering an integrated approach to anomaly detection.

- **Deep Clustering-based Fair Outlier Detection (DCFOD) (Chawla & Gionis, 2013):** Enhances outlier detection with a focus on fairness, combining deep clustering and adversarial training for representation learning.

D.2.7. Representation-based Models

- **Deep Support Vector Data Description (DeepSVDD) (Ruff et al., 2018):** Minimizes the volume of a hypersphere enclosing network data representations, isolating anomalies outside this sphere.

- **Deep Isolation Forest for Anomaly Detection (DIF) (Xu et al., 2023):** Utilizes deep learning to enhance traditional isolation forest techniques, offering improved anomaly detection in complex datasets with minimal parameter tuning.

Each method's unique mechanism and application context provide a rich landscape of techniques for unsupervised anomaly detection, illustrating the field's diverse methodologies and the breadth of approaches to tackling anomaly detection challenges.

D.3. Supplementary Experimental Results

In the appendix, we detail the statistical analysis conducted to compare the performance of various anomaly detectors. We obtained this diagram by conducting a Friedman test (p-value: 4.657e-19), indicating significant differences among different detectors. We utilized average ranks and the Nemenyi test to generate the critical difference diagram, as shown in Figure 5. It is noteworthy that the vector version exhibits significantly superior performance compared to the scalar version across more methods. The detailed outcomes for the AUCROC and AUCPR metrics, spanning 30 datasets and against 17 baseline approaches, are showcased in Table 5 and Table 6.

D.3.1. Degrees of Freedom in t-Distribution

In fixed degrees of freedom scenarios, specifically when set to 1, the benefits of utilizing the t-distribution become less pronounced. Drawing from existing literature (Xie et al., 2016; Van Der Maaten, 2009), the flexibility to learn the degrees of freedom or to perform cross-validation on the validation set is particularly pertinent in unsupervised contexts. For the sake of simplicity and to minimize computational demands, we opted to maintain the degrees of freedom at 1, which provided robust performance while reducing complexity.

Table 5: AUCROC of 17 unsupervised algorithms on 30 tabular benchmark datasets. In each dataset, the algorithm with the highest AUCROC is marked in red, the second highest in blue, and the third highest in green.

Dataset	SOD	HBOS	PCA	OC SVM	LOF	KNN	LODA	IForest	DA GMM	ECOD	COPOD	DB SCAN	CBLOF	DCOD	KMeans--	Deep SVDD	DIF	UniCAD (Scalar)	UniCAD (Vector)
annthyroid	77.38	60.15	66.24	57.23	70.20	71.69	41.02	82.01	56.53	78.66	76.80	50.08	62.28	55.01	64.99	76.09	66.76	75.27	72.72
backdoor	68.77	71.56	80.16	85.04	85.79	80.58	66.38	72.15	55.98	86.08	80.97	76.55	81.91	79.57	89.11	78.83	92.87	87.28	89.24
breastw	93.97	98.94	95.13	80.30	40.61	97.01	98.49	98.32	N/A	99.17	99.68	85.20	96.86	99.02	97.05	63.36	77.45	98.15	98.56
campaign	69.16	78.55	72.78	65.70	59.04	72.27	51.67	71.71	56.03	76.10	77.69	50.60	64.34	63.16	63.51	54.42	67.53	73.52	73.64
celeba	48.44	76.18	79.38	70.70	38.95	59.63	60.17	70.41	44.74	76.48	75.68	50.36	73.99	91.41	56.76	45.17	65.29	81.38	82.00
census	62.12	64.89	68.74	54.90	47.46	66.88	37.14	59.52	59.65	67.63	69.07	58.50	60.17	72.84	63.33	54.16	59.66	67.90	67.84
glass	73.36	77.23	66.29	35.36	69.20	82.29	73.13	77.13	76.09	65.83	72.43	54.55	78.30	78.07	77.30	55.71	84.57	79.52	82.17
Hepatitis	67.83	79.85	75.95	67.75	38.06	52.76	64.87	69.75	54.80	75.22	82.05	68.12	73.05	48.38	64.64	57.45	74.24	75.53	80.62
http	78.04	99.53	99.72	99.59	27.46	3.37	12.48	99.96	N/A	98.10	99.29	49.97	99.60	99.53	99.55	60.38	99.49	99.53	99.52
Ionosphere	86.37	62.49	79.19	75.92	90.59	88.26	78.42	84.50	73.41	73.15	79.34	81.12	90.79	57.78	91.36	53.94	89.74	92.04	90.37
landsat	59.54	55.14	35.76	36.15	53.90	57.95	38.17	47.64	43.92	36.10	41.55	50.17	63.69	33.40	55.31	62.48	54.84	49.60	57.37
Lymphography	71.22	99.49	99.82	99.54	89.86	55.91	85.55	99.81	72.11	99.52	99.48	74.16	99.81	81.19	100.00	71.91	83.67	99.29	99.73
mnist	60.10	60.42	85.29	82.95	67.13	80.58	72.27	80.98	67.23	74.61	77.74	50.00	79.96	65.23	82.45	50.98	88.16	86.00	86.64
musk	74.09	100.00	100.00	80.58	41.18	69.89	95.11	99.99	76.85	95.40	94.20	50.00	100.00	42.19	72.16	66.02	98.22	99.92	100.00
pendigits	66.29	93.04	93.73	93.75	47.99	72.95	89.10	94.76	64.22	93.01	90.68	55.33	96.93	94.33	94.37	27.32	93.79	95.12	95.52
Pima	61.25	71.07	70.77	66.92	65.71	73.43	65.93	72.87	55.93	63.05	69.10	51.39	71.49	72.16	70.44	49.49	67.28	75.16	74.87
satellite	63.96	74.80	59.62	59.02	55.88	65.18	61.98	70.43	62.33	58.09	63.20	55.52	71.32	55.97	67.71	57.40	74.52	72.46	77.65
satimage-2	83.08	97.65	97.62	97.35	47.36	92.60	97.56	99.16	96.29	96.28	97.21	75.74	99.84	86.01	99.88	55.68	99.63	99.87	99.88
shuttle	69.51	98.63	98.62	97.40	57.11	69.64	60.95	99.56	97.92	99.13	99.35	50.40	93.07	97.20	69.97	51.81	97.00	99.15	98.75
skin	60.35	60.15	45.26	49.45	46.47	71.46	45.75	68.21	N/A	49.08	47.55	50.00	68.03	64.34	65.47	45.69	66.36	72.26	69.69
Stamps	73.26	90.73	91.47	83.86	51.26	68.61	87.18	91.21	88.89	87.87	93.40	52.08	69.89	93.41	79.78	59.48	87.95	91.37	94.18
thyroid	92.81	95.62	96.34	87.92	86.86	95.93	74.30	98.30	79.75	97.94	94.30	53.57	94.74	78.55	92.26	52.14	96.26	97.66	97.48
vertebral	40.32	28.56	37.06	37.99	49.29	33.79	30.57	36.66	53.20	40.66	25.64	49.74	41.01	38.13	38.14	37.81	47.20	33.11	47.37
vowels	92.65	72.21	65.29	61.59	93.12	97.26	70.36	73.94	60.58	62.24	53.15	57.50	92.12	51.56	93.45	49.87	81.02	88.38	92.09
Waveform	68.57	68.77	65.48	56.29	73.32	73.78	60.13	71.47	49.35	62.36	75.03	66.41	71.27	63.47	74.35	53.94	75.33	71.81	74.29
WBC	94.60	98.72	98.20	99.03	54.17	90.56	96.91	99.01	N/A	99.11	99.11	87.43	96.88	94.92	97.45	62.46	81.27	97.68	98.93
Wilt	53.25	32.49	20.39	31.28	50.65	48.42	26.42	41.94	37.29	36.30	33.40	49.96	34.50	44.71	34.91	45.90	39.46	48.95	52.56
wine	46.11	91.36	84.37	73.07	37.74	44.98	90.12	80.37	61.70	77.22	88.65	40.33	27.14	82.18	27.36	64.26	41.69	82.72	95.25
WPBC	51.28	51.24	46.01	45.35	41.41	46.59	49.31	46.63	47.80	46.65	49.34	52.22	45.32	49.67	45.01	44.01	44.69	48.02	49.90
Avg. Rank	**11.00**	**8.26**	**8.98**	**11.59**	**13.59**	**10.00**	**13.24**	**7.09**	**13.24**	**9.19**	**8.29**	**14.21**	**8.07**	**10.90**	**8.71**	**15.48**	**8.38**	**5.41**	**3.59**

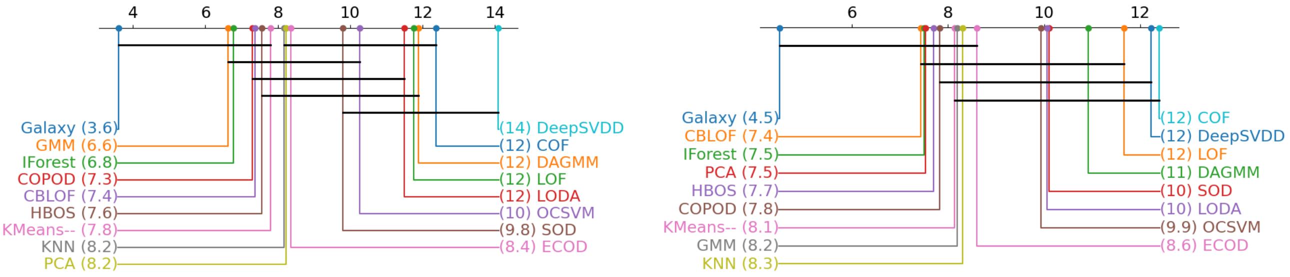

(a) AUC-ROC

(b) AUC-PR

Figure 5: Critical difference diagrams for AUC-ROC and AUC-PR.

D.3.2. Ablation Study on Hyperparameter Settings

An ablation study was conducted to evaluate the impact of hyperparameters k and l. A grid search was performed over various values of these hyperparameters across 30 datasets, benchmarking against 17 baseline methods. The comprehensive results, showcasing average ranks based on AUC-ROC, are summarized in the following table:

The findings indicate that the method exhibits robustness across specific parameter ranges. To ensure fair comparisons, a consistent parameter set ($k = 10, l = 1\%$) was applied, demonstrating strong performance across the majority of datasets.

Additionally, guidelines for selecting hyperparameters were examined. While techniques such as the elbow method and silhouette coefficient were considered for determining the optimal number of clusters, they proved to be time-consuming and exhibited weak correlation with anomaly detection performance. An ensemble learning approach, which involved random searches of k values and aggregation of anomaly scores, showed promise in enhancing performance and model robustness for certain datasets. Future research will further explore this area.

D.4. Complexity Analysis

The complexity of each iteration in UniCAD involves three parts: constructing the outlier set, updating the network parameters Θ, and optimizing the mixture model using the EM algorithm. Constructing the outlier set requires a sorting

Table 6: AUCPR of 17 unsupervised algorithms on 30 tabular benchmark datasets. In each dataset, the algorithm with the highest AUCPR is marked in red, the second highest in blue, and the third highest in green.

Dataset	SOD	HBOS	PCA	OC SVM	LOF	KNN	LODA	IForest	DA GMM	ECOD	COPOD	DB SCAN	CBLOF	DCOD	KMeans--	Deep SVDD	DIF	UniCAD (Scalar)	UniCAD (Vector)
annthyroid	18.84	16.99	16.12	10.37	15.71	16.74	7.06	30.47	9.64	25.35	16.58	7.60	13.74	10.01	15.41	21.75	18.93	26.37	25.03
backdoor	37.07	4.96	31.29	8.79	26.14	44.37	13.84	4.75	5.47	10.72	7.69	21.04	7.03	6.77	15.47	55.70	41.46	37.77	36.36
breastw	84.88	97.71	95.11	82.70	28.55	92.19	97.04	96.04	N/A	98.54	99.40	78.42	91.94	96.83	92.25	48.60	50.65	94.47	95.90
campaign	19.14	38.01	27.90	29.25	14.59	27.18	14.11	32.26	14.54	36.65	38.58	11.43	20.88	19.61	18.86	16.75	26.52	27.66	27.12
celeba	2.36	13.82	15.89	10.73	1.73	3.14	4.04	8.96	1.95	13.96	13.69	2.32	11.22	17.48	3.19	2.73	5.44	15.12	14.66
census	8.54	8.68	10.02	6.82	5.48	9.04	5.03	7.78	9.03	9.46	9.92	7.52	7.52	10.92	8.13	8.42	7.42	9.70	9.75
glass	18.73	11.82	10.05	8.02	20.11	20.26	13.37	10.99	24.58	15.35	9.78	6.88	11.57	9.66	14.66	8.46	18.86	13.29	15.33
Hepatitis	24.73	37.73	36.65	29.44	13.67	21.95	30.90	26.25	22.93	32.80	41.50	22.31	36.54	19.53	25.14	30.04	34.93	36.08	43.37
http	8.32	44.79	56.43	46.86	3.82	0.70	0.67	90.83	N/A	16.61	35.19	0.37	47.53	44.03	45.09	13.39	41.72	43.53	43.52
Ionosphere	85.88	41.78	73.92	74.54	88.07	90.41	73.04	80.41	64.97	64.69	69.89	63.04	89.77	47.63	91.36	43.24	87.45	89.55	87.61
landsat	26.38	22.03	16.18	16.21	24.69	24.65	18.86	19.81	24.48	16.24	17.48	20.80	31.05	15.57	22.40	36.92	24.35	20.84	23.27
Lymphography	22.00	91.83	97.02	93.59	23.08	38.69	44.54	97.31	19.52	90.87	88.68	7.66	97.31	12.34	100.00	34.58	32.84	91.69	96.66
mnist	19.15	12.51	39.93	33.20	20.90	35.53	25.86	27.71	23.75	17.45	21.35	9.21	30.60	23.59	37.12	20.18	44.55	41.19	41.94
musk	7.59	100.00	99.89	10.61	2.82	9.65	47.60	99.61	32.76	50.13	34.79	3.16	100.00	2.87	37.55	8.78	70.70	97.65	99.96
pendigits	4.46	29.27	23.65	23.52	3.78	6.50	18.71	26.05	4.67	30.65	21.22	2.94	32.87	22.21	32.67	1.53	23.75	24.86	21.68
Pima	48.24	56.61	54.03	50.00	47.18	55.14	44.09	55.82	41.55	50.45	55.19	36.65	52.99	50.24	53.50	35.02	46.34	54.66	54.23
satellite	47.23	67.25	59.64	57.61	37.68	50.01	61.94	65.92	58.33	52.22	56.58	37.56	61.43	43.31	54.68	41.77	68.92	71.68	75.13
satimage-2	26.11	78.04	85.69	82.71	4.30	39.14	80.52	93.45	22.07	64.49	76.55	12.08	97.09	8.12	97.13	2.58	72.90	97.33	97.31
shuttle	20.27	96.40	92.35	85.29	13.76	20.38	48.75	97.62	93.20	90.45	96.56	7.68	79.89	81.82	32.66	12.41	67.23	92.05	92.36
skin	24.61	23.70	17.40	19.03	18.25	28.72	18.44	26.08	N/A	18.37	17.99	20.89	28.34	26.29	25.58	19.06	25.36	28.87	28.72
Stamps	20.28	35.24	41.09	31.39	21.29	23.53	34.60	39.49	43.73	33.21	43.10	11.03	24.46	47.36	35.63	12.07	34.68	42.39	50.94
thyroid	23.56	50.98	44.34	21.23	20.81	34.98	14.68	63.11	16.06	51.06	19.64	9.44	29.88	10.56	31.69	2.70	50.36	60.99	60.06
vertebral	11.79	9.23	10.49	10.94	14.24	10.57	9.68	10.46	15.24	11.84	8.89	13.11	11.43	11.58	10.54	10.62	14.31	9.78	12.96
vowels	38.88	13.41	8.92	8.24	34.42	63.41	13.82	15.12	12.22	10.56	4.14	13.27	35.14	3.58	49.10	4.58	14.97	26.52	32.42
Waveform	9.66	5.86	5.79	4.37	11.33	13.04	4.71	6.24	3.11	4.76	6.90	5.33	17.93	4.26	19.74	4.41	11.28	6.49	7.83
WBC	54.00	73.56	82.29	89.87	5.57	66.55	78.67	90.49	N/A	86.19	86.19	30.25	67.31	33.43	71.88	8.99	13.32	68.69	83.14
Wilt	5.53	3.84	3.13	3.62	5.05	4.73	3.36	4.23	4.00	3.93	3.69	5.33	3.74	4.62	3.76	4.65	4.05	4.80	5.19
wine	7.95	43.08	30.87	21.56	7.77	8.43	48.82	25.96	17.51	23.54	45.71	8.11	5.98	24.44	6.27	18.78	8.38	21.40	49.59
WPBC	25.62	23.04	23.01	22.93	20.29	21.49	25.39	22.42	22.49	21.24	22.81	23.86	21.08	22.86	20.58	25.00	20.73	22.71	24.90
Avg. Rank	**10.83**	**8.19**	**8.31**	**11.14**	**13.24**	**9.36**	**11.79**	**7.29**	**11.96**	**9.36**	**9.53**	**14.91**	**8.53**	**11.97**	**9.03**	**13.41**	**9.10**	**6.31**	**4.74**

Table 7: Learning vs. Fixed Degrees of Freedom

Metric	Learn v	Fix $v = 1$
AUC-ROC Avg. Rank	4.4	3.34
AUC-PR Avg. Rank	5.05	4.47

Table 8: Results of Hyperparameter Grid Search

$l \backslash k$	10	20	30	40
0.01	3.34	4.31	4.69	4.71
0.05	4.44	4.23	4.65	4.88
0.10	4.27	4.46	4.48	4.88

operation, for which we use Numpy's built-in quantile calculation with a time complexity of $\mathcal{O}(N \log N)$. Considering the number of network parameters along with the computation of the loss function, the computational complexity for optimizing Θ is approximately $\mathcal{O}(TNDd + TNKd)$. The EM algorithm for the Student's t mixture model includes two main steps: the E-step, where the complexity for computing the probability (or responsibility) of each data point belonging to each component is approximately $\mathcal{O}(NKd)$, and the M-step, where the full computational complexity of updating the parameters (mean, covariance matrix) of each component is $\mathcal{O}(NKd^2)$. In practice, we use diagonal covariance matrices, which reduces the update complexity to roughly $\mathcal{O}(NKd)$. If the EM algorithm requires T round to converge, its time complexity is approximately $\mathcal{O}(TNKd)$. Therefore, the time complexity for t-iterations is $\mathcal{O}(tN(\log N + Td(D + K)))$.